Journal of Sciences, Islamic Republic of Iran 20(1): 41-53 (2009) http://jsciences.ut.ac.ir
University of Tehran, ISSN 1016-1104

Source of Cement in the Great Oolite Reservoir, Storrington Oil Field, Weald Basin, South of England

G. Mirab Shabestari,[1,*] R.H. Worden,[2] and J.D. Marshall[2]

[1]*Department of Geology, Faculty of Sciences, University of Birjand, Birjand, Islamic Republic of Iran*
[2]*Department of Earth and Ocean Sciences, University of Liverpool, Liverpool, United Kingdom*

Received: 12 March 2008 / Revised: 6 December 2008 / Accepted: 30 December 2008

Abstract

The source of cement in oilfields is critical to the prediction of the distribution of cements in the reservoirs and also prediction of reservoir quality. The source of mineral forming cements has been determined for the Storrington oolitic carbonate reservoir (Middle Jurassic Great Oolite Formation, Weald Basin, onshore UK) using a combination of petrography, electron microscopy, fluid inclusion analysis, atomic absorption spectrometry and stable isotopes analysis techniques. Petrographic interpretations revealed that ferroan calcite cement is the most significant diagenetic mineral and has a major control on reservoir quality. The preferred conclusion from this study is that the Great Oolite reservoir has acted as closed system during early diagenesis and has performed as open system during burial diagenesis. Also, elements for burial diagenetic cements have been sourced from neighbouring formation. Finally, stable isotopes analysis demonstrated that the dominant source of carbon in the Great Oolite reservoir is marine and is derived from the rock itself.

Keywords: Great Oolite Formation; Storrington Oilfield; Oolitic reservoirs; Carbonate reservoir diagenesis

Introduction

The aim of this study is to investigate about these fundamental problems: (i) Are burial diagenetic cements in carbonate reservoirs internally sourced from within the reservoir or do they come from external sources? (ii) If external sources are important, are they from neighbouring (sandstone, mudstone) formations or have they been resulted from long range transport from external sources?

These questions are important since they strongly affect the assessment and importance of neighbouring rock units on carbonate diagenesis and cementation and also assessment of the relationship between regional fluid movement and diagenesis. The results can assist us in prediction of the distribution of cements in the reservoirs and also prediction of reservoir quality evolution during burial diagenesis.

The case study in this paper is the Great Oolite reservoir in Storrington oil field. The Storrington oil field is geographically situated immediately west of the small town of Storrington (approximately 20 Km NW of Brighton), on the western flank of the Weald Basin (Fig. 1). The Weald Basin is located in southeast England and

* Corresponding author, Tel.: +98(561)2502148, Fax: +98(561)2502041, E-mail: gshabestari@birjand.ac.ir

forms an easterly extension to the Wessex Basin. The Weald basin was a depositional centre during the Jurassic and Cretaceous periods. Inversion of the basin in the Early Tertiary formed the Weald Anticline, which represents the expression of basin at outcrop [12,29,30].

The structure is an East-West trending elongated anticline nearly 6 Km long, with a fault seal to the north and south and dip closure elsewhere. The structure has a relief of about 50-70 m above the spill point along the eastern nose [20]. The oil-water contact is transitional and the free water level is placed at 1370 m (TVDSS) (Fig. 2). The reservoir in the Storrington field is the Middle Jurassic (Bathonian) oolitic grainstones and packstones of the Great Oolite Formation and the Oxford Clay (Upper Jurassic) acts as the seal. Storrington petroleum is thought to be sourced by secondary migration from deeper, breached traps during Tertiary uplift of the basin [4, 25].

The Great Oolite Formation was deposited in a broad, shallow-water carbonate shoal complex overlying an axis of early Middle Jurassic tectonic uplift that linked the London-Brabant and Welsh Massifs [9, 26, 28]. The Great Oolite Formation in the Storrington field has been divided into three units (Fig. 3). This division was based on corrolatable groupings of oolites separated by periods of relative deepening and/or temporary cessation of ooid production characterised by a widespread increase in lime mud content [17]. The Lower Oolites are grey to grey-buff, poorly sorted, shelly and skeletal packstones and overlies basinal shales/shaley mudstones of the Fullers Earth. Ooids and bioclasts are the most common allochems and occur in equal proportions throughout [23]. The Lower Oolites represent the initial development and progradation of the shoal belt into the Storrington area. The Middle Oolite unit represents the main environment of ooid formation and is reflected by less abundant shelly and skeletal material. These sediments consist of a succession of thickly bedded, buff to light-buff porous oolitic grainstones that are typically cross-bedded. Ooids are the dominant particles throughout the unit. The Middle Oolites represent a stacked sequence of high-energy oolitic grainstones, which developed in shallow water [23]. The Upper Oolites comprise a sequence of coarse-grained shelly and skeletal oolites with thin shelly claystone interbeds. Ooids and bioclasts are the most common allochems and one or other of these grain types tends to dominate. Intraclasts and peloids occur but are not widespread. Muddy laminae occur and muddy/clayey drapes are present. The Upper Oolites are the result of renewed progradation of the shoal belt re-established oolite-dominated sedimentation in the Storrington area [23].

Materials and Methods

In this study, two wells in Storrington field were sampled. A relatively high spatial resolution core sampling strategy was undertaken in Storrington-2 well. Additional core samples were collected from Storrington-1 well. Fourty-eight samples were taken throughout the whole reservoir facies (the Great Oolite Formation) in the Storrington field, between the depths of 1296 m and 1365 m in Storrington-2 well and the depth of 1276 m and 1344 m in Storrington-1 well (all depths in the paper are cited as true vertical depth sub-sea = TVDSS). All analyses were carried out at the laboratories of the Department of Earth and Ocean Science/University of Liverpool, UK.

The petrographic investigation was carried out on stained acetate peels and on unstained microprobe sections. The probe sections were impregnated with blue epoxy resin to aid identification of porosity. Petrographic analysis was initially carried out on the stained acetate peels because textures, differences in carbonate iron content, etc., were more visible than in probe sections. Chosen Samples for analysis were examined using a Jeol WINSEM 6400 scanning electron microscope (SEM) equipped with a secondary electron and backscattered electron detector [15, 37].

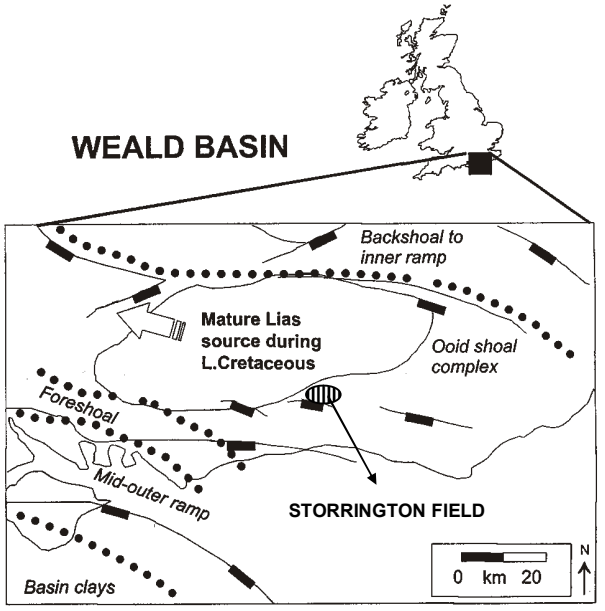

Figure 1. Regional location map of the Storrington oil field with generalised Great Oolite facies belts from Sellwood *et al.* [26] and area of mature Liassic source rock indicated.

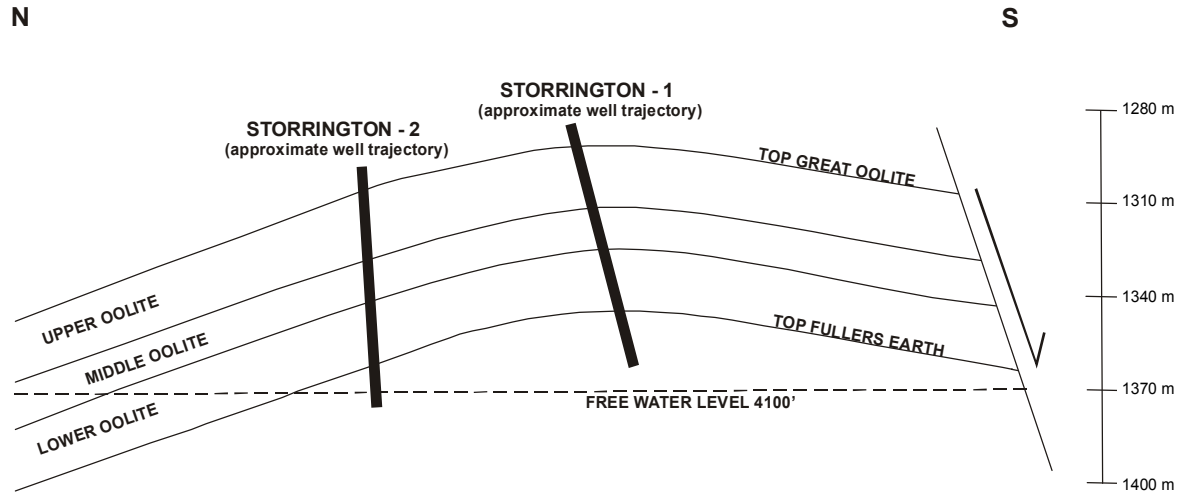

Figure 2. Schematic cross-section of the Storrington field, free water level at 1370 m (TVDSS) [23].

Distribution of minor elements (Fe, Mg, Mn and Sr) was determined by atomic absorption analysis. Iron, magnesium, manganese and strontium were detected in samples with a Perkin Elmer Atomic Absorption Spectrometer (model 3100).

All core samples were sub-sampled and prepared for whole rock isotope analysis. In addition, isotope analysis was carried out on different cement types. The CO_2 released by the reaction was separated cryo-genically and analysed by stable isotope ratio mass spectrometry using a VG SIRA-12 mass spectrometer. Isotope data are reported in standard notation as per mil (‰) deviations relative to the V-SMOW (Standard Mean Ocean Water) and PDB (Pee Dee belemnite) standards. Reproducibility, based on repeated analysis of internal carbonate standards was ±0.01 for both $\delta^{13}C$ and $\delta^{18}O$.

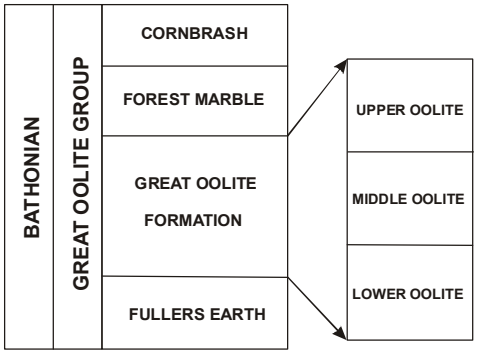

Figure 3. Stratigraphy of the Great Oolite Formation in the Storrington area (modified after McLimans and Videtich [17]).

Examination and analysis of fluid inclusions were made on four 100μm thick doubly polished wafers from wells ST-1 and ST-2. Optical examination and micro-thermometry was carried out using a Nikon 2-Pol polarising microscope. The following microscope objectives were used: x40 (normal lens) and x100 (normal lens). Micro-thermometry was carried out using a Linkam THMSG 600 heating-cooling stage attached to a Linkam PR600 heating controller and Linkam CS196 cooling controller attached to the microscope. The coolant used in each case was liquid nitrogen.

Results

1. Petrology

The rock fabric and mineralogy of the Great Oolite Formation in Storrington were determined using petrographic analysis of peels and examination of polished probe sections for analysis of pore systems. SEM was used to examine the relationship between grain types and detailed analysis of mineral relationships and microporosity.

1.1. Facies Descriptions

Based on petrographic analysis, the reservoir unit was divided into three different facies. Facies 1 consisted of an oolitic grainstone. This facies had >70% ooids and <10% micrite (plus non-ferroan dolomite). Facies 2 was split up into sub-facies 2a and 2b. Both sub-facies are bioclast rich, however sub-facies 2b is an echinoderm rich and sub-facies 2a is an echinoderm poor. Facies 3 was a micrite rich facies and consisted of >40% micrite and non-ferroan dolomite.

1.2. Detrital Components

Ooids and peloids. Ooids were the dominant grains noted and the ooid cortex is often micritised (Fig. 4a). Ooids were originally developed around skeletal or peloidal nuclei. The ooids often appear crushed or deformed. Ooids were originally high-Mg calcite and were leached out during diagenesis to result in microporous ooids. Preservation of radial fabrics in ooids near skeletal material in which aragonite has been dissolved, suggests that the ooids were originally Mg-calcite [17]. Peloids are also present as a minor component and are apparently structureless micritic grains.

Bioclastic material. Various types of fragmental bioclastic were observed (Fig. 4b). This skeletal debris consists mainly of echinoderm plates, brachiopod, molluscan, such as bivalves and gastropods, and bryozoans. Other less common bioclastic consisted of forams and rare solitary coral fragments. Some moldic porosity was preserved and this was mostly in the Middle Oolite unit, but much of the pores have been destroyed by subsequent precipitation of calcite cement. Echinoderm fragments are especially common in the Middle Oolites.

Micrite. Micrite is treated as a depositional component of each facies (Fig. 4b), although it is acknowledged that some may have been of eogenetic origin. Micrite occurs mainly in facies 3 and is locally replaced by non-ferroan dolomite.

1.3. Cement Types

Marine cement. This type of cement forms bladed crystals protruding out from the edges of grains and bioclastic material. It is present in extremely minor abundances. It occurs as isopachous palisades of generally 10-20μm long, high-Mg calcite compared to aragonite as it does not have the typical acicular, needle-like morphology of aragonite (Fig. 4a).

Non-ferroan calcite. Isopachous non-ferroan and pore filling equant non-ferroan calcite were both present in the Storrington reservoir. This cement type is not volumetrically abundant. Sparry equant non-ferroan calcite grows out into pore space on top of isopachous cement. This type of cement is more abundant and is volumetrically significant cement phase.

Syntaxial cement. Syntaxial overgrowths grew particularly on echinoderm fragments are predominantly of non-ferroan calcite, but show some chemical zonation towards Fe-rich composition at crystal edges adjacent to pores. This cement is not volumetrically significant. Syntaxial cement is more abundant in the Middle Oolite unit than the Upper and Lower Oolites (Fig. 4c).

Non-ferroan dolomite. Non-ferroan dolomite in Storrington occurs as microrhombs (40-50μm) replacing a locally argillaceous micrite matrix. This dolomite is frequently noted in muddy drapes. Non-ferroan dolomite replaces micrite in the matrix and is therefore more common in facies 3 than the other facies. In the Upper and Lower Oolites, the micrite matrix has been locally, almost completely replaced by a mosaic of fine rhombic crystals. Parts of ooids have also been replaced by this dolomite.

Ferroan calcite. Ferroan calcite cement in the Great Oolite at Storrington is coarsely crystalline (approximately 50-100μm) (Fig. 4a). Two phases of ferroan calcite exist. Ferroan calcite phase 1 pre-dates saddle dolomite and ferroan calcite phase 2 post-dates saddle dolomite precipitation. Ferroan calcite displays blocky and equigranular fabrics and is sometimes present as peripheral zones on syntaxial crystals. This cement is most common in the Upper and Lower Oolites and is not particularly abundant in the Middle Oolite unit. Intergranular ferroan calcite is, on average, more abundant in sub-facies 2a than facies 1, 2b and 3.

Saddle dolomite. Saddle dolomite is not a common mineral phase in the Storrington field, but occurs preferentially in the Upper and Lower Oolite units. It is coarsely crystalline, approximately 80-110μm, and grows into pores (Fig. 4d). Saddle dolomite is rarely replaced by ferroan calcite (dedolomitisation) and also replaces parts of ooids and bioclastic material.

2. Geochemical Analysis

2.1. Elemental Analysis

Distribution of iron, manganese, strontium and magnesium are shown in Figure 5. All the values are presented in ppm.

Iron. Figure 5a shows iron (ppm) plotted as a function of depth. Average data for the Upper, Middle and Lower units are shown in Table 1a. Iron shows an average decrease from 4891±5530 ppm in the Upper Oolite unit to an average of 3607±2855 ppm in the Middle Oolite unit and increases to an average of 6685±2554 ppm in the Lower Oolite unit. The Upper Oolite unit also shows on average less iron than Lower Oolite unit (Table 1a). Average data for each of the facies is given in Table 1b. Facies 3 contains the greatest amount of iron (6250±3727 ppm). Facies 1 contains the least amount of iron (2964±267 ppm).

Manganese. Figure 5b shows manganese (ppm) plotted as a function of depth. Manganese decreases from an average of 228±63 ppm in the Upper Oolite unit to an average of 175±34 ppm in the Middle Oolite unit and increases to an average of 382±56 ppm in the

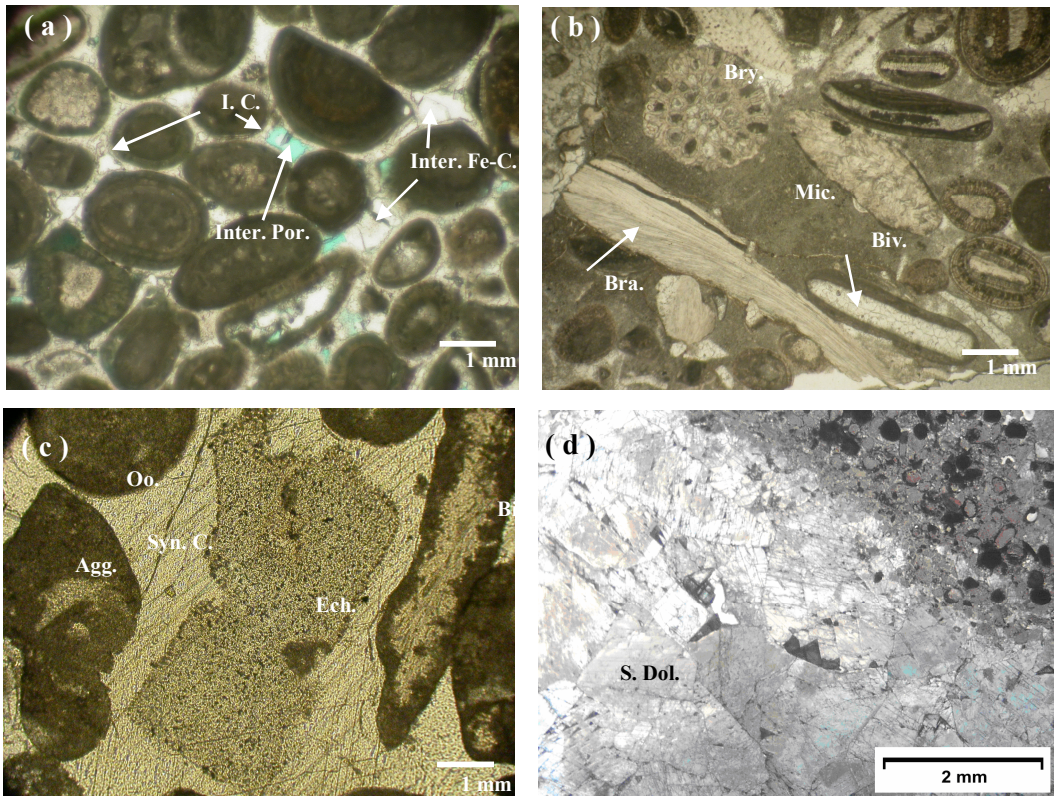

Figure 4. (a) Polished thin section photomicrograph (plain light) of an oolitic grainstone sample showing isopachous calcite cement (I. C.), intergranular Fe-calcite cement (Inter. Fe-C.) and intergranular macroporosity (Inter. Por.). Sample ST2-11, 1322.1 m (TVDSS), Storrington-2 well. (b) Polished thin section photomicrograph (plain light) of a bioclastic packstone sample showing bryozoan (Bry.) and brachiopod (Bra.) bioclasts and replaced bivalve shell (Biv.) which is the core of an ooid within micritic matrix (Mic.). Sample ST1-4, 1298.3 m (TVDSS), Storrington-1 well. (c) Polished thin section photomicrograph (plain light) of syntaxial overgrowth cement (Syn. C.) around an echinoderm bioclast (Ech.) which is closely surrounded by other fragments such as ooid (Oo.), aggregate (Agg.) and bivalve shell (Biv.). Sample ST1-10, 1326.8 m (TVDSS), Storrington-1 well. (d) Stained peel photomicrograph of saddle dolomite (S. Dol.) crystals. Sample ST2-32, 1355.0 m (TVDSS), Storrington-2 well.

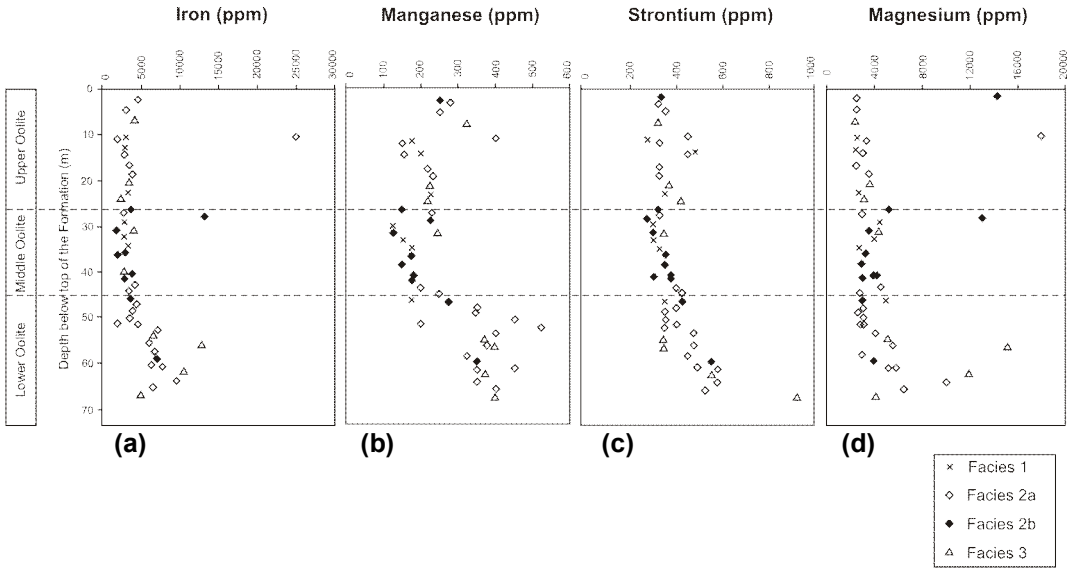

Figure 5. (a) Iron (ppm) (bulk chemical data) vs. depth, all facies. (b) Manganese (ppm) (bulk chemical data) vs. depth, all facies. (c) Strontium (ppm) (bulk chemical data) vs. depth, all facies. (d) Magnesium (ppm) (bulk chemical data) vs. depth, all facies.

Table 1. Average bulk chemical data for: (a) Upper, Middle and Lower Oolite units; (b) facies 1, sub-facies 2a, sub-facies 2b and facies 3 (n: Number of samples)

		n	Mg (ppm)	Fe (ppm)	Mn (ppm)	Sr (ppm)
a	Upper Oolite	19	4597.2 ± 4308.1	4736.1 ± 5218.4	227.8 ± 62.9	358.3 ± 54.9
	Middle Oolite	14	4384.6 ± 2693.8	3711.5 ± 2943.6	176.9 ± 36.0	344.2 ± 48.0
	Lower Oolite	15	5635.3 ± 3554.5	6685.3 ± 2554.0	382.4 ± 56.4	480.3 ± 142.1
b	Facies 1	8	3428.6 ± 1048.0	2964.3 ± 267.3	175.0 ± 32.3	339.2 ± 65.9
	Sub-facies 2a	20	3470.5 ± 3489.1	5665.9 ± 4754.8	312.5 ± 103.7	414.3 ± 81.1
	Sub-facies 2b	11	5477.3 ± 4093.4	4704.5 ± 3431.1	202.3 ± 66.6	359.1 ± 76.1
	Facies 3	9	6343.8 ± 4650.1	6250.0 ± 3727.3	321.9 ± 77.3	456.3 ± 202.6

Lower Oolite unit. Average manganese data show a decrease in the Middle Oolite unit (Table 1a) compared to the Upper and Lower Oolite units. The Upper Oolite unit also shows on average less manganese than the Lower Oolite unit. Table 1b shows average data for each of the four facies. Facies 2b and facies 3 contain the greatest amounts of manganese (5477±4093 ppm and 6343±4650 ppm respectively).

Strontium. Figure 5c shows strontium (ppm) plotted as a function of depth. Strontium also shows a minor increase with depth. Strontium decreases from an average of 480±142 ppm in the Upper Oolite unit to an average of 346±47 ppm in the Middle Oolite unit and increases to an average of 382±54 ppm in the Lower Oolite unit (Table 1a). Average sums of strontium all show a decrease in the Middle Oolite unit. Table 1b gives average data for strontium in each of the four facies. Strontium shows an increase in facies 2a (414.3±81.1 ppm) and facies 3 (546.3±202.6 ppm) compared to facies 1 (339.2±65.9 ppm) and facies 2b (359.1±76.1 ppm).

Magnesium. Figure 5d shows magnesium (ppm) plotted as a function of depth. Magnesium decreases from an average of 4597±4308 ppm in the Upper Oolite unit to an average of 4385±2694 ppm in the Middle Oolite unit and increases to an average of 5635±3555 ppm in the Lower Oolite unit (Table 1a). Average sums of magnesium all show a decrease in the Middle Oolite unit. The Upper Oolite unit also shows, on average, less magnesium than the Lower Oolite unit. Table 1b gives average data for magnesium in each of the four facies. Magnesium shows an increase in facies 2b (5477±4093 ppm) and facies 3 (6343±4650 ppm) compared to facies 1 (3428±1048 ppm) and facies 2a (3470±3489.1 ppm).

2.2. Isotope Data

Carbon and oxygen isotope ratio measurements were carried out on physically separated ferroan calcite and saddle dolomite. Whole rock measurements were also carried out for all core samples. The results of these analyses are given in Tables 2 and 3. Figure 6 shows that whole rock $\delta^{13}C$ data range from a maximum of +2.1‰ to a minimum of +0.6‰ and also reveals $\delta^{13}C$ data from ferroan calcite and saddle dolomite. This plot shows that saddle dolomite has slightly more negative $\delta^{13}C$ signatures than ferroan calcite. $\delta^{13}C$ data for ferroan calcite are slightly less positive in the Lower Oolite unit. Average ferroan cement abundances are also indicated. Fig. 7 shows a cross plot of $\delta^{13}C$ vs. $\delta^{18}O$.

The most negative $\delta^{18}O$ values correspond to the lightest $\delta^{13}C$ values. Saddle dolomite shows the lightest $\delta^{13}C$ and the most negative $\delta^{18}O$ values. However all $\delta^{13}C$ values of both whole rock and separate cements are slightly depleted. Figure 8 shows $\delta^{18}O$ values of the fluid from which the intergranular ferroan calcite may have precipitated. This figure shows that the fluid had an average $\delta^{18}O$ value of +5.0‰ (±0.01‰). Figure 9 presents the calculated average $\delta^{18}O$ value of the fluid responsible for precipitation of saddle dolomite. This figure indicates the average $\delta^{18}O$ value for the fluid to be +0.2‰ (±0.01‰). Interpretation of this data will be discussed in the next section. Figure 10 illustrates the calculated $\delta^{18}O$ values for the fluid which precipitated fracture fill ferroan calcite. The fluid which precipitated fracture fill ferroan calcite had an average $\delta^{18}O$ value of +1.4‰ (±0.01‰) at an average temperature of 60°C.

Discussion

Sources of Cement

Ferroan calcite cement has a major control on both porosity and permeability in the Storrington oil field. It is therefore important to establish the conditions under which this cement was precipitated. Both carbon ($\delta^{13}C$) and oxygen ($\delta^{18}O$) isotopes were used to determine the source of dissolved carbon and the fluid type at the time of precipitation.

Table 2. Isotope data ($\delta^{13}C$ and $\delta^{18}O$) for ferroan calcite and saddle dolomite cements from Storrington-1 and Storrington-2 wells

Well	Sample	Depth (m) (TVDSS)	Mineral	Sampling Point	$\delta^{18}O$ (‰PDB)	$\delta^{13}C$ (‰PDB)
Storrington-1	ST1-4	1298.3	Fe-Calcite	Intergranular	-6.5	1.4
	ST1-5	1302.8	Fe-Calcite	Intergranular	-9.7	0.9
	ST1-11	1331.4	Fe-Calcite	Intergranular	-4.6	1.3
	ST1-12	1332.7	Fe-Calcite	Fracture	-7.5	1.5
	ST1-12	1332.7	Fe-Calcite	Fracture	-8.5	1.6
Storrington-2	ST2-1	1297.4	Dolomite	Intergranular	-10.1	-0.1
	ST2-1	1297.4	Dolomite	Intergranular	-11.6	-0.1
	ST2-9	1316.6	Fe-Calcite	Intergranular	-7.8	1.4
	ST2-9	1316.6	Fe-Calcite	Fracture	-7.7	1.4
	ST2-9	1316.6	Fe-Calcite	Intergranular	-7.0	1.6
	ST2-21	1339.0	Fe-Calcite	Intergranular	-7.5	1.7
	ST2-22	1340.3	Fe-Calcite	Intergranular	-6.2	0.9
	ST2-24	1343.3	Fe-Calcite	Fracture	-6.7	1.6
	ST2-25	1344.2	Fe-Calcite	Intergranular	-5.8	1.6
	ST2-27	1347.5	Fe-Calcite	Intergranular	-5.8	1.7
	ST2-28	1348.8	Fe-Calcite	Fracture	-6.0	1.4
	ST2-29	1350.4	Fe-Calcite	Intergranular	-9.0	1.0
	ST2-32	1355.0	Fe-Calcite	Intergranular	-4.6	1.3
	ST2-37	1362.8	Fe-Calcite	Fracture	-7.6	0.3

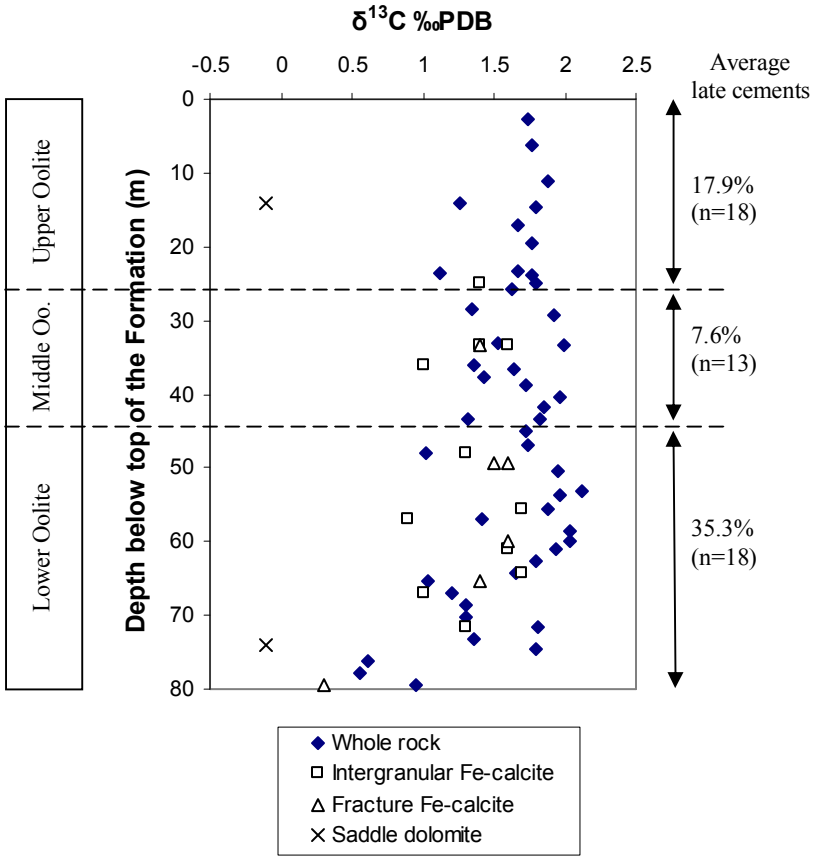

Figure 6. ^{13}C isotope data for whole rock, intergranular Fe-calcite, fracture-filling Fe-calcite and saddle dolomite samples plotted as a function of depth.

Potential sources of carbon for CO_3^{2-} during burial diagenesis are: (1) organic derived CO_2; and (2) dissolution within the rock itself. Carbon is distributed between the rock and the pore water (HCO_3^-) of reservoirs. The relative reservoir sizes are discordant with the rock reservoir being dominant [18], thus in diagenetic systems where significant water-rock interaction has occurred, the isotopic composition of the carbon tends to be dominated by the average composition of rocks in equilibrium with the pore waters.

If metastable carbonates of primary marine composition are actively driving cementation through their dissolution, pore water $\delta^{13}C$ will converge towards original marine compositions [1,2]. In contrast, dissolved bicarbonate derived from decomposition of organic matter, generally not a reservoir of significant size can produce local perturbations in pore water carbon composition, largely because of contribution of extremely light carbon [18, 33].

Analysis of whole rock $\delta^{13}C$ signatures suggests a shift from an initial $\delta^{13}C$ of ~+2.1‰ (thought to be typical of Mid-Jurassic seawater) to a $\delta^{13}C$ of +0.6‰ (Fig. 11). The lightest $\delta^{13}C$ values occur in separate cement data for saddle dolomite in the Storrington reservoir (-0.01‰). Although the majority of the extracted cement data fall within the range of +1.6‰ to -0.01‰ (for ferroan calcite and saddle dolomite) which is within the realm of marine derived carbon, a minor contribution of organic derived CO_2 may also contribute as a source in the burial cements. Isotopes analyses were carried out on both ferroan calcite and saddle dolomite and previous evidence [7] has shown that saddle dolomite was precipitated during maximum burial. However, ferroan calcite was precipitated during deep burial and uplift. This means that a mixture of sources of carbon may also be present as there was no way to physically separate out ferroan calcite phase 1 and phase 2 during these analyses. This also means that the marine signature would dominate any indication of an organic carbon source. However, both whole rock data and separate cement data appear to trend towards lighter $\delta^{13}C$ values (Fig. 6). An organic source has also been invoked by other workers. Prezbindowski [24] showed that burial ferroan calcite cements fell within the range of 0.0 to -1.0‰ can be attributed to thermal alteration of associated organic material which is going to be the source of organic carbon incorporated in the calcite cement. Sun *et al.* [27] also suggested that the decrease in $\delta^{13}C$ and $\delta^{18}O$ may indicate a more light carbon input with progressive burial and increasing temperature from the increasing influence of organic matter. $\delta^{13}C$ values in this study ranged from +0.07‰ to +3.18‰ for saddle dolomite. Meyers and Lohmann [18] showed that cements with carbon isotope values of +2.4‰ had a mixed source of carbon from crinoid carbon and organic

Table 3. Isotope data ($\delta^{13}C$ and $\delta^{18}O$) for whole rock samples from Storrington-1 and Storrington-2 wells

Well	Sample	Depth (m) (TVDSS)	$\delta^{18}O$ (‰PDB)	$\delta^{13}C$ (‰PDB)
Storrington-1	ST1- 1	1286.0	-4.26	1.74
	ST1- 2	1289.7	-4.21	1.77
	ST1- 3	1294.4	-3.5	1.88
	ST1- 4	1298.3	-4.05	1.8
	ST1- 5	1302.8	-4.48	1.36
	ST1- 6	1307.0	-4.6	1.12
	ST1- 7	1311.7	-5.17	1.34
	ST1- 8	1316.5	-5.51	1.53
	ST1- 9	1321.1	-5.09	1.43
	ST1- 10	1326.8	-4.74	1.32
	ST1- 11	1331.4	-6.4	1.02
Storrington-2	ST2- 1	1297.4	-2.61	1.26
	ST2- 2	1298.1	-4.6	1.8
	ST2- 3	1300.4	-4.45	1.67
	ST2- 4	1303.0	-4.54	1.77
	ST2- 5	1306.5	-4.68	1.67
	ST2- 6	1307.2	-4.52	1.77
	ST2- 7	1309.1	-4.67	1.63
	ST2- 8	1312.7	-4.89	1.92
	ST2- 9	1316.6	-3.68	1.99
	ST2- 10	1319.9	-3.72	1.64
	ST2- 11	1322.1	-5.38	1.72
	ST2- 12	1323.8	-4.91	1.97
	ST2- 13	1325.1	-5.07	1.85
	ST2- 14	1326.7	-5.23	1.82
	ST2- 15	1328.3	-4.8	1.72
	ST2- 16	1330.3	-4.67	1.74
	ST2- 18	1333.8	-3.76	1.95
	ST2- 19	1336.4	-3.28	2.12
	ST2- 20	1337.1	-3.52	1.97
	ST2- 21	1339.0	-3.39	1.88
	ST2- 22	1340.3	-5.6	1.42
	ST2- 23	1342.0	-3.42	2.03
	ST2- 24	1343.3	-3.21	2.03
	ST2- 25	1344.2	-3.28	1.93
	ST2- 26	1345.9	-4.09	1.8
	ST2- 27	1347.5	-3.95	1.66
	ST2- 28	1348.8	-3.79	1.04
	ST2- 29	1350.4	-4.33	1.2
	ST2- 30	1352.0	-6.29	1.3
	ST2- 31	1353.7	-4.94	1.3
	ST2- 32	1355.0	-4.16	1.81
	ST2- 33	1356.6	-5.65	1.36
	ST2- 34	1357.9	-5.81	1.8
	ST2- 35	1359.5	-4.49	0.61
	ST2- 36	1361.1	-4.32	0.56
	ST2- 37	1362.8	-4.65	0.95

soil carbon (approximately 8% assuming the organic carbon had a $\delta^{13}C$ of about ~-25‰). Carbonate cements in deeply buried sandstones show a wide range of $\delta^{13}C$ values [15, 19]. The $\delta^{13}C$ associated with organic carbon may well have been buffered by the surrounding limestone and the overwhelming marine signature would certainly dilute the $\delta^{13}C$ value. Figure 5a shows that whole rock data get progressively slightly lighter with depth. Abundant late sparry calcite probably has an important influence on the bulk isotopic composition of limestones [10]. This pattern in Storrington is probably dominated by the presence of burial ferroan calcite (Fig. 6).

The oxygen isotopic composition of burial calcite and dolomite cements are clearly affected by temperature-dependant fractionation of oxygen isotopes between cement and fluid [3, 8, 21]. Figure 7 reveals that saddle dolomite exhibits a more negative range of oxygen value than calcite. Fracture filling ferroan calcite and intergranular ferroan calcite exhibit a similar range of oxygen values implying a similar temperature range of formation.

Stable isotope fractionation curves were used to calculate the $\delta^{18}O$ of the pore waters, which led to the precipitation of ferroan calcite [5] and saddle dolomite [13, 22] (eq. 1 and 2):

$$1000 \ln \alpha_{calcite-water} = (2.78\times10^{6}\times T^{-2}) - 2.89 \quad \text{(eq. 1)}$$

$$1000 \ln \alpha_{dolomite-water} = (3.34\times10^{6}\times T^{-2}) - 3.34 \quad \text{(eq. 2)}$$

Where,

$1000 \ln \alpha_{mineral-water}$ = oxygen − isotope mineral water fractionation factor

T = Temperature in degrees Kelvin

Minimum, mean and maximum fluid inclusion temperatures (homogenisation temperatures) were used to calculate the $\delta^{18}O$ range of the waters present at the time of precipitation of both ferroan calcite and saddle dolomite. Figures 8, 9 and 10 show the $\delta^{18}O$ range of water for intergranular ferroan calcite, fracture filling ferroan calcite and saddle dolomite respectively. Figure 8 shows that fluid responsible for precipitation of intergranular calcite has a mean $\delta^{18}O$ (SMOW) value of +5.0‰ (±0.01‰) at a mean temperature of 81.9°C. Figure 9 indicates that the fluid responsible for precipitating saddle dolomite has a mean $\delta^{18}O$ (SMOW) value of +0.2‰ (±0.01‰). These data show that as burial progressed, the pore waters became enriched in $\delta^{18}O$ due to water-rock interaction demonstrated by intergranular ferroan calcite data. Following this pore-water evolution path, saddle dolomite was precipitated at maximum burial depth. Figure 10 shows that the mean $\delta^{18}O$ (SMOW) signature for fracture filling

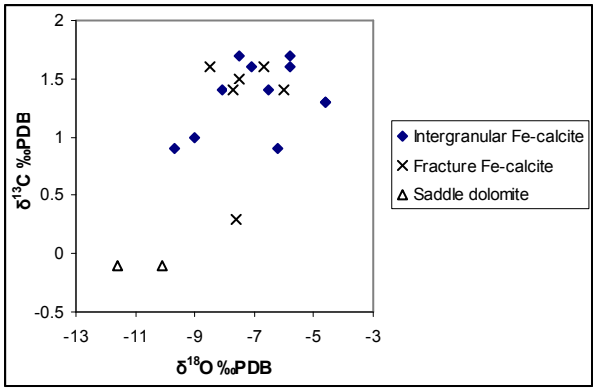

Figure 7. Carbon versus oxygen isotopes data for ferroan calcite (fracture+intergranular) and saddle dolomite samples.

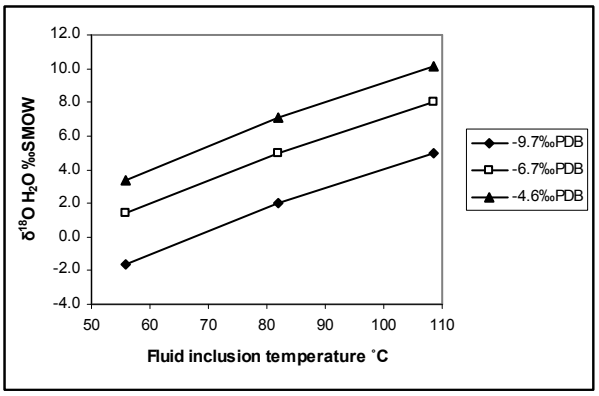

Figure 8. ^{18}O water data for intergranular ferroan calcite. Temperature = from fluid inclusion data. Range = taken from 50 to 110 degrees.

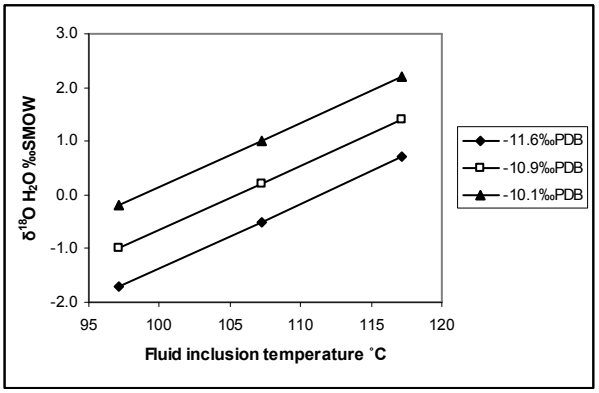

Figure 9. Fractionation curves for $\delta^{18}O$ of the fluid from which saddle dolomite precipitated, temperatures = range from 97.1 to 117.2 degrees and are homogenisation temperatures measured from primary 2-phase aqueous inclusions within saddle dolomite.

ferroan calcite at a mean temperature of 60°C is +1.4‰ (±0.01‰). The temperature range chosen for the precipitation of fracture filling ferroan calcite is a best estimate range based on the fact that dedolomitisation is predominantly seen in fractures and therefore much of the second phase of ferroan calcite (which replaces saddle dolomite) occurs in fractures. Fluid inclusion temperatures ranged between 55°C and 110°C. However, this range is for both ferroan calcite phase 1 and ferroan calcite phase 2. A time-temperature plot shows that ferroan calcite phase 2 was likely to be precipitated during uplift and cooling and thus it is likely to be precipitated from lower temperatures than ferroan calcite phase 1. It is likely that the $\delta^{18}O$ data of the waters show a pore water evolution path from intergranular ferroan calcite (phase 1), to saddle dolomite (at maximum burial) to fracture filling ferroan calcite (phase 2). The period of uplift during the Early Tertiary may have allowed minor influx of meteoric water at this time. The preferred interpretation is that the fracture filling calcite was precipitated from a brine with a minor input of meteoric water. Intergranular ferroan calcite (phase 1) was likely precipitated from a saline brine as was saddle dolomite. The output for these calculations can be seen in Tables 4, 5 and 6.

Distribution of Elements (Fe, Mg, Mn and Sr)

The distribution and sources of iron, magnesium, manganese and strontium are also examined. Figure 5a shows that iron increases downwards in the Lower Oolite unit. Iron also shown an increase at the top of the Middle Oolite unit, this also corresponds to an increase in magnesium (Fig. 5d) and both these distributions reflect a high saddle dolomite abundance at this depth. Iron, magnesium and manganese show an increase near to the top of the Upper Oolite unit. The distribution pattern of these elements provides important information about the source. The distribution of iron, magnesium and manganese demonstrates that these three elements increase towards the clay rich sequences of the Forest Marble/Lower Cornbrash above and the Fullers Earth Formation below (this distribution pattern is a reflection of the increase in ferroan calcite (Fe) and saddle dolomite (Fe+Mg) in this unit).

The potential of basinal shale to serve as a source of Ca, Fe, Mg, Na and Si during deep burial diagenesis is well documented in the literature. Numerous workers [6, 7, 14, 16] have proposed that the burial diagenetic transformation of smectite to illite is accompanied by the release of metal ions to the pore fluid. The smectite-illite transformation can take place over the temperature range of 50°C to 125°C (burial depths of 2 to 4 Km with

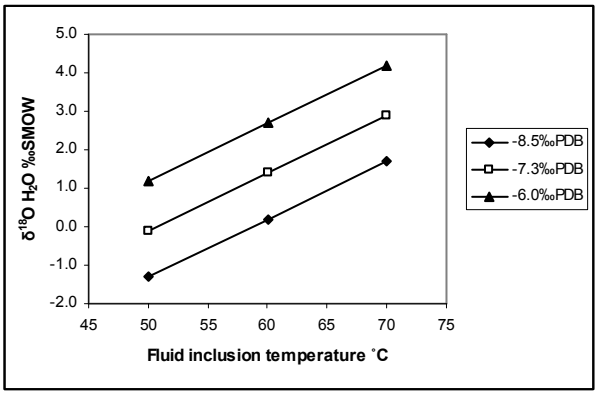

Figure 10. Fractionation curves for $\delta^{18}O$ of the fluid from which fracture fill ferroan calcite precipitated, temperatures = range from 50 to 70 degrees and are homogenisation temperatures measured from primary 2-phase aqueous inclusions within ferroan calcite.

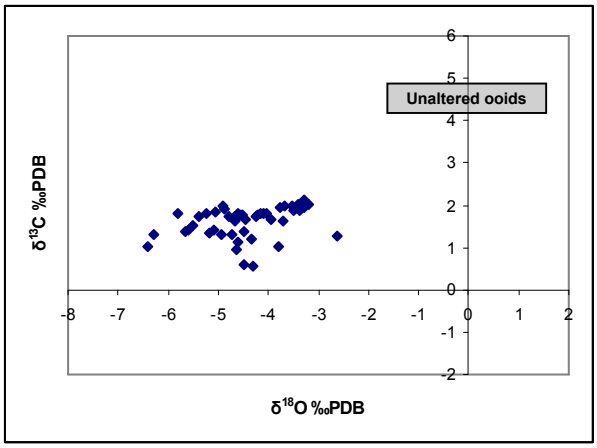

Figure 11. Crossplot of $\delta^{18}O$ versus $\delta^{13}C$ (Whole rock isotopes) (Unaltered ooids from Sellwood *et al.* [26]).

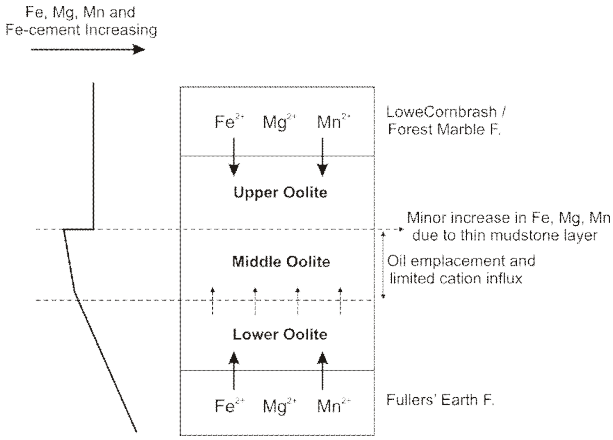

Figure 12. Showing sources of Mg, Fe, Mn and Sr in the Storrington reservoir and effect of timing of oil emplacement on import of these elements.

normal geothermal gradients). Previously published burial history graph [20] has shown that the Fullers Earth (below the Great Oolite) would have reached temperatures within this range where the smectite-illite transformation reaction takes place.

Manganese occurs in greater proportions in the Upper and Lower Oolite units (Fig. 5b). This is also due to the greater abundance of burial cement in these two units. The greater abundance of iron, magnesium and manganese in the Lower Oolite unit compared to the Upper Oolite unit reflects the increased abundance of saddle dolomite in this unit compared to the Upper Oolite unit.

It is concluded that the source of iron, manganese and possible some magnesium is external and was provided from the Fullers Earth Formation underlying the main reservoir interval and the Lower Cornbrash /Forest Marble overlying the main reservoir interval (Fig. 12).

One piece of evidence for supply of Mg and Fe from clay/mudstone intervals comes from the anomalously high saddle dolomite value and magnesium value at the top of the Middle Oolite unit. This sample is situated 27 m below the top of the Great Oolite Formation at the Middle Oolite and Upper Oolite boundary. In Storrington-2 a thin alumino-silicate mudstone band is located at this boundary. Thus this mudstone band may have acted as a source of magnesium and iron, accounting for the abundance of saddle dolomite at this depth. The proposed mechanism of element source and transport in the Storrington reservoir is diffusion. The process of element import can be seen in Figure 12.

Figure 5c shows the distribution of strontium. Strontium shows an increase from the top of the Middle Oolite unit to the bottom of the Lower Oolite unit. To explain this distribution of strontium it is necessary to look at the source of this trace element in calcite cement. Sources of strontium may be: (1) marine waters and carbonates; (2) meteoric water: meteoric water (which is commonly involved in transformation of aragonite to calcite and calcite recrystallisation) contains negligible strontium; and (3) detrital allumino-silicate minerals: sandstone beds.

The most obvious source of strontium in the Great Oolite would be dissolution of aragonite bioclastic material. Aragonite typically contains 8000 to 10000 ppm strontium [19]. Dissolution of bioclastic material would have liberated a source of strontium. Bivalves and gastropods were commonly composed of aragonite skeletons. Strontium concentrations (although still low) are greater in the Upper and Lower Oolite units (maximum of 500 ppm) compared to the Middle Oolite unit. These two units also contain the greatest abun

Table 4. Output data generated from fluid inclusion temperatures and oxygen isotope data for ferroan calcite. (55.8°C = minimum temperature, 81.9°C = mean temperature and 108.6°C = maximum temperature from fluid inclusion temperature range)

Fluid inclusion temperature (°C)	$\delta^{18}O$ water (min.) (‰SMOW)	$\delta^{18}O$ water (mean) (‰SMOW)	$\delta^{18}O$ water (max.) (‰SMOW)
55.8	-1.6	1.4	3.4
81.9	2.0	5.0	7.1
108.6	5.0	8.0	10.1

Table 5. Output data generated from fluid inclusion temperatures and oxygen isotope data for saddle dolomite. (97.1°C = minimum temperature, 107.2°C = mean temperature and 117.2°C = maximum temperature from fluid inclusion temperature range) (data based on two measurements)

Fluid inclusion temperature (°C)	$\delta^{18}O$ water (min.) (‰SMOW)	$\delta^{18}O$ water (mean) (‰SMOW)	$\delta^{18}O$ water (max.) (‰SMOW)
97.1	-1.7	-1.0	-0.2
107.2	-0.5	0.2	1.0
117.2	0.7	1.4	2.2

Table 6. Output data generated from fluid inclusion temperatures and oxygen isotope data for fracture filling ferroan calcite. (50°C = minimum temperature, 60°C = mean temperature and 70°C = maximum temperature from fluid inclusion temperature range) (data based on two measurements)

Fluid inclusion temperature (°C)	$\delta^{18}O$ water (min.) (‰SMOW)	$\delta^{18}O$ water (mean) (‰SMOW)	$\delta^{18}O$ water (max.) (‰SMOW)
50	-1.3	-0.1	1.2
60	0.2	1.4	2.7
70	1.7	2.9	4.2

dance of bioclastic material (sub-facies 2a). Abundant bioclastic material may have sourced strontium in subsequent cements. Most ancient limestones have only a few hundred parts per million Sr [31] mainly due to the loss of strontium during neomorphic processes such as transformation of aragonite to calcite and calcite recrystallisation.

In conclusion: - The source of early meteoric cement in Storrington oil field is commonly dissolution of bioclastic material calcite. The source of magnesium in early shallow burial dolomite was likely to be from seawater and stabilisation of high Mg-calcite ooids and

bioclastic material.

- The reservoir has probably acted as *closed system* during early diagenesis. Magnesium and calcium carbonate were retained and redistributed during diagenesis.

- The reservoir acted as *open system* during burial diagenesis to a limited degree. Iron and manganese both influxed the reservoir during burial diagenesis and were probably sourced from the Fullers Earth, Hesters Copse (below the reservoir unit) and Forest Marble/Lower Cornbrash Formations (above the reservoir unit). In the Storrington reservoir, the distance of the Middle Oolite unit from the source of manganese and iron may have been a minor control on the distribution of these two species.

- Source of carbon in ferroan cements in the Great Oolite reservoir was dominantly internal and was derived from the rock itself.

Acknowledgments

We would like to thank Star Energy Ltd at Humbly Grove oilfield (Hampshire) and British Geological Survey at Keyworth (Nottinghamshire) for providing core and materials to work on. Also, thanks should go to the Ministry of Science, Research and Technology of the Islamic Republic of Iran and the University of Birjand for financial support.

References

1. Allan J.R. and Matthews R.K. Carbon and oxygen isotopes as diagenetic and stratigraphic tools: data from surface and subsurface of Barbados, West Indies. *Geology*, **5**, 16-20 (1977).
2. Allan J.R. and Matthews R.K. Isotope signatures associated with meteoric diagenesis. *Sedimentology*, **29**, 797-817 (1982).
3. Anderson J.H. and Arthur M.A. Stable isotopes of oxygen and carbon and their application to sedimentologic and palaeoenvironmental problems. In: Arthur M.A. (Ed.), *Stable Isotopes in Sedimentary Geology*, SEPM Short Course, **10**, 1.1-1.151 (1983).
4. Butler M. and Pullan C.P. Tertiary structures and hydrocarbon entrapment in the Weald Basin of southern England. In: Hardman R.F.P. and Brooks J. (Eds.), *Tectonic Events responsible for Britain's Oil and Gas Reserves*, Geological Society Special Publication, **55**, 371-391 (1991).
5. Freidman I. and O'Neil J.R. Compilation of stable isotope fractionation factors of geochemical interest. In: Fleischer M. (Ed.), *Data of Geochemistry*, sixth edition, United States Geological Survey Professional Paper 440-kk, 12p. (1977).
6. Gregg J.M. Regional epigenetic dolomitisation in the Bonneterre dolomite (Cambrian), southern Missouri. *Geology*, **13**, 503-506 (1985).
7. Heasley E.C., Worden R.H. and Hendry J.P. Cement distribution in a carbonate reservoir: recognition of a palaeo oil-water contact and its relationship to reservoir quality in the Humbly Grove field, onshore UK. *Marine and Petroleum Geology*, **17**, 639-654 (2000).
8. Hendry J.P. Geochemical trends and palaeohydrological significance of shallow burial calcite and ankerite cements in Middle Jurassic strata on the East Midland Shelf (onshore UK). *Sedimentary Geology*, **151**, 149-176 (2002).
9. Hesselbo S.P. Sequence stratigraphy and inferred relative sea-level change from the onshore British Jurassic. *Proceeding of the Geologists' Association#119,* **16**, 19-34 (2007).
10. Hudson J.D. Carbon isotopes and limestone cement. *Geology*, **6**, 19-22 (1975).
11. Krinsley D.H., Pye K. and Kearsley A.T. Application of backscattered electron microscopy in shale petrology. *Geological Magazine*, **120**, 109-114 (1983).
12. Lake S.D. and Karner G.D. The structure and evolution of the Wessex Basin, southern England: an example of inversion tectonics. *Tectonophysics*, **137**, 347-378 (1987).
13. Land L.S. The application of stable isotopes to studies of the origin of dolomite and to problems of diagenesis of clastic sediments. In: *Stable Isotopes in Sedimentary Geology*. Society of Economic Palaeontologists and Mineralogists, Short course **10**, 4.1-4.22 (1983).
14. Lee M.R. and Freidman G.M. Deep burial dolomitisation in the Ordovician Ellenberger Group carbonates, West Texas and southeastern New Mexico. *Journal of Sedimentary Petrology*, **58**, 910-913 (1987).
15. Longstaffe F.J. Stable isotopes as tracers in clastic diagenesis. In: Hutcheon I.E. (Ed.), *Short course in burial diagenesis*, Mineralogical Association of Canada, short course series, **15**, 201-277 (1986).
16. McHargue T.R. and Price R.C. Dolomite from clay in argillaceous or shale-associated marine carbonates. *Journal of Sedimentary Petrology*, **52**, 873-886 (1982).
17. McLimans R.K. and Videtich P.E. Reservoir diagenesis and oil migration: Middle Jurassic Great Oolite Limestone, Wealden Basin, Southern England. In: Brooks J. and Glennie K.W. (Eds.), *Petroleum Geology of North West Europe*, Graham and Trottman, London, 119-128 (1987).
18. Meyers W.J. and Lohmann K.C. Isotope geochemistry of regionally extensive calcite cement zones and marine components in Mississippian limestones, New Mexico. In: Scheidermann N. and Harris P.M. (Eds.), *Carbonate cements*, Society of Economic Palaeontologists and Mineralogists, Special Publication, **36**, 241-264 (1985).
19. Miliken K.L., Land L.S. and Loucks R.G. History of burial diagenesis determined from isotopic geochemistry, Frio Formation, Texas. *American Association of Petroleum Geologists Bulletin*, **65**, 1397-1413 (1981).
20. Mingard H. Preliminary report on the Geology and Petrophysics of the Storrington oil/gas discovery. *Report URL/P205b/GEO/041/*, SOCO Oil Onshore Ltd., UK (1989).
21. Morad S., Worden R.H. and Ketzer J.M. Oxygen and hydrogen isotopic composition of diagenetic clay

minerals in sandstones: a review of the data and controls. In: Worden R.H. and Morad S. (Eds.), *Clay Mineral Cements in Sandstones*, International Association of Sedimentologists' Special Publication, **34**, 63-91 (2003).
22. O'Neil J.R. and Epstein S. Oxygen isotope fractionation in the system dolomite-calcite-carbon dioxide. *Science*, **152**, 198-201 (1966).
23. Poroperm-Geochem Sedimentological and reservoir evaluation of cores 2-5 from Storrington#1. *Report 1703*, WOO1/12 (1986).
24. Prezbindowski D.R. Burial cementation-is it important? A case study, Stuart City trend, south central Texas. In: Scheidermann N. and Harris P.M. (Eds.), *Carbonate cements*, Society of Economic Palaeontologists and Mineralogists, Special Publication, **36**, 241-264 (1985).
25. Scotchman I.C., Carr A.D., Astin T.R. and Kelly J. Pore fluid evolution in the Kimmeridge Clay Formation of the UK outer Moray Firth: Implications for sandstone diagenesis. *Marine and Petroleum Geology*, **19**, 247-273 (2002).
26. Sellwood B.W., Scott J., Mikkelsen P. and Akroyd P. Stratigraphy and sedimentology of the Great Oolite Group in the Humbly Grove Oilfield, Hampshire. *Marine and Petroleum Geology*, **2**, 44-55 (1985).
27. Sun S.Q., Fallick A.E. and Williams B.P.J. Influence of original fabric on subsequent porosity evolution: an example from the Corallian (Upper Jurassic) reefal limestones, the Weald Basin, southern England. *Sedimentary Geology*, **79**, 139-160 (1992).
28. Taylor S.P. and Sellwood B.W. The context of low-stand events in the Kimmeridgian (Late Jurassic) sequence sratigraphic evolution of the Wessex-Weald Basin, Southern England. *Sedimentary Geology*, **151**, 89-4106 (2002).
29. Taylor S.P., Sellwood B.W., Gallois R.W. and Chambers M.H. A sequence stratigraphy of the Kimmeridgian and Bolonian stages (Late Jurassic): Wessex-Weald Basin, Southern England. *Journal of the Geological Society of London*, **54**, 179-192 (2001).
30. Trueman S. The Humbly Grove, Herriard, Storrington, Singleton, Stockbridge, Goodworth, Horndean, Palmers Wood, Bletchingley and Albury Fields, Hampshire, Surrey and Sussex, UK onshore; Part 9: Weald and Wessex Basins Fields. *Geological Society of London Memoirs*, **20**, 929-941 (2003).
31. Veizer J. and Demovic R. Strontium as a tool in facies analysis. *Journal of Sedimentary Petrology*, **44**, 93-115 (1974).
32. White S.H., Shaw H.F. and Huggett J.M. The use of back-scattered electron imaging for the petrographic study of sandstone and shales. *Journal of Sedimentary Petrology*, **54**, 487-494 (1984).
33. Zeng J., Bai G. and Peng J. Possible effects of carbonate content in source rock on fluid composition and chemical reaction - A preliminary result of simulation. *Journal of Geochemical Exploration*, **89**, 450-454 (2006).